J Solid State Electrochem (2010) 14:1565–1575
DOI 10.1007/s10008-009-0981-4

ORIGINAL PAPER

Capacitive characteristics of nanocomposites of conducting polypyrrole and functionalized carbon nanotubes: effects of in situ dopant and film thickness

Jie Wang · Youlong Xu · Feng Yan · Jianbo Zhu · Jingping Wang · Fang Xiao

Received: 9 July 2009 / Revised: 15 October 2009 / Accepted: 17 November 2009 / Published online: 16 December 2009

Abstract The nanocomposites of functionalized single-walled carbon nanotubes (FSWNTs) and conducting polypyrrole (PPy) doped by FSWNTs, Cl^-, toluenesulfonate (TOS^-), and dodecylbenzenesulfonate (DBS^-), respectively, were electrochemically co-deposited to evaluate their applicability in supercapacitors. The effects of the dopants, with focus on their mass, size and surfactivity, and film thickness on the capacitive characteristics were investigated in 3 M KCl aqueous solution. Although the nanostructure of composites can admittedly improve the capacitive properties, dopant anion was demonstrated to be a more essential factor. The specific capacitance of PPy-TOS/FSWNT nanocomposites was greater than that of pristine PPy/FSWNT nanocomposites and PPy-DBS/FSWNT nanocomposites by ten and 100 times, respectively. Furthermore, PPy-TOS/FSWNT nanocomposites exhibited the lowest dependence of capacitance on the charging–discharging rate and composite thickness due to its high electronic and ionic conductivity resulting from the appropriate doping level and size of TOS^- as well as the synergic effect of PPy-TOS and FSWNTs. In addition, PPy-TOS/FSWNT nanocomposites presented a remarkably stable cycling performance.

Keywords Polypyrrole · Nanocomposites · Dopant · Thickness · Supercapacitors

J. Wang · Y. Xu (✉) · F. Yan · J. Zhu · J. Wang · F. Xiao
Electronic Materials Research Laboratory,
Key Laboratory of the Ministry of Education,
Xi'an Jiaotong University,
Xi'an 710049, China
e-mail: ylxuxjtu@mail.xjtu.edu.cn

Introduction

The great interest in the development of energy sources to support peak power for the devices from portable equipment to electric vehicles has significantly stimulated the research of electrochemical capacitors (also known as supercapacitors) [1–3]. Electronically conducting polymers (ECPs) have been widely studied as electrode materials of supercapacitors due to their advantages including high capacitance compared with high-surface carbon materials, low cost in comparison with noble metal oxides, and easy synthesis by chemical and electrochemical methods [4–7]. Among ECPs, polypyrrole (PPy) [8–11] has attracted much attention due to its additional outstanding characteristics such as good stability both in water and atmosphere and environmental friendliness [12]. Besides, its charging–discharging process can proceed in neutral electrolytes, which are much less corrosive to most materials than the strongly acidic solution (e.g., H_2SO_4) employed by carbon materials and conducting polyaniline. These advantages promote the applicability of PPy in supercapacitors [11]. However, the fast-response ability and high specific capacitance of PPy, as well as of other ECPs, were generally achievable only in thin films because of low ionic mobility within the solid polymer. From a practical appoint of view, thicker layers of electroactive material are required to improve energy per area of electrode in order to achieve higher energy density of supercapacitors.

An effective strategy to obtain thick film with high electroactivity is to prepare the highly porous composites of PPy and carbon nanotubes (PPy/CNTs), which are considered as an ideal electrode material in terms of electronic conductivity, specific surface area, and ionic transport

throughout the internal volume of the electrode via the interconnected pore structure. The electrochemical capacitance properties of PPy/CNT composites have been wildly studied in the last decade [12–20], since Wan et al. [21] reported that PPy/CNT composites can be synthesized by chemical method. Compared with the chemical one, the electrochemical method has a number of advantages. The most important one is that composite films can be directly produced on the current collector and naturally integrated as continuous uniform films, saving the use of a binder that is often an insulator and hydrophobic, such as PTFE. This is one reason that the capacitance performance of polymer/CNTs prepared by the electrochemical method is generally better than that by the chemical one [22].

In addition, the thickness of films can be easily controlled by the quantity of polymerization charge. Therefore, electrochemical route has been intensively used to prepare polymer-based electrode materials of supercapacitors. According to the available literature, two electrochemical routes are used to prepare PPy/CNTs composites. One is to electrochemically synthesize PPy on the CNTs matrix which was pre-deposited on an electrode substrate by adsorption [23]. It is difficult to obtain uniform polymer films on CNTs surfaces using this route, also called two-step method, because the outer layers of the CNT matrix contain much more polymer than the inner ones due to bulk diffusion [19]. The other route is to electrochemically co-deposit (ECD) PPy with CNTs into a composite coating on an electrode in a thin layer of ionic liquid solution [19] or in a suspension of CNTs and pyrrole monomer [24]. The feasibility of the ECD method in the latter solution is demonstrated by Chen et al. [13], where the CNT suspension can be obtained by either acid treatment of CNTs to make them anionic or by grafting functional groups to the CNTs surface [25, 26]. We reported that the homogenous composite electrodes of PPy/FSWNTs for supercapacitors can be prepared by ECD method in stable colloidal aqueous solution of functionalized single-walled carbon nanotubes (FSWNTs) achieved by synchronously cutting and functionalizing SWNTs in concentrated sulfuric and nitric acid [18]. This is the approach followed in this present study.

The charging–discharging process of polymer electrodes is actually a doping–dedoping process, and the dopant has an inevitable impact on the electrochemical capacitance properties of PPy films. Song et al. [9] reported that PPy doped by ClO_4^- have a higher specific capacitance than PPy doped by NO_3^- do. Hu et al. [10] found that the PPy films doped by Cl^- with polymerization charges equal to or less than 1 Ccm^{-2} exhibit ideal capacitive characteristics with a high specific capacitance of 268 Fg^{-1} (based on the mass of PPy). Ingram et al. [11] reported that PPy ladder-doped with polysulfonated aromatic anions have a very fast charging–discharging ability and a high specific capacitance of 160 Fg^{-1} (based on the actual weights of electrode material). It can be concluded that the dopant is a key factor to capacitance properties of PPy films [27]; however, there is no literature available about the effect of doping ions on the electrochemical capacitance of PPy/FSWNT nanocomposites.

This study aimed at investigating the effects of the dopant in terms of mass, size and surfactivity, and the film thickness on electrochemical capacitance properties of PPy/FSWNT nanocomposites. The performance of electrochemically co-deposited PPy/FSWNT nanocomposites, doped individually by FSWNTs and additionally by three other typical kinds of anions in terms of mass, size, and surfactivity: Cl^-, toluenesulfonate (TOS^-), and dodecylbenzenesulfonate (DBS^-), respectively, was compared to evaluate their applicability in supercapacitors. The mechanism of ion diffusion in the composite during charging–discharging process was discussed by using electrochemical impedance spectroscopy (EIS) technology. The effects of doping anions on the morphology of the composites were examined by field emission scanning electron microscope, and the structure of PPy in the composites was characterized by X-ray photoelectron spectroscopy (XPS).

Experimental

Pyrrole monomer (Py; Fluka, 99%) was distilled before use. SWNTs (purity of CNTs>90%, content of SWNTs>60%, diameter<5 nm, length 0.5–2 μm) were purchased from Shenzhen Nanotech Port Co., Ltd, and were functionalized by being suspended in concentration H_2SO_4/HNO_3 (volume ratio 3/1) solution and sonicated for 12 h in water bath. The product FSWNTs were separated from the mixed acid solution by repetitious centrifugation with a rotate speed of 12,000 rpm in a high-speed filter centrifugal (TG16-WS, Shanghai Lu XiangYi Centrifuge Instrument Co., Ltd) until the aqueous media of FSWNTs reached neutrality. PPy/FSWNT composites were galvanostatically prepared on tantalum electrodes (1 cm×1 cm) in aqueous dispersive solution of 0.1 wt.% FSWNTs and 0.3 M Py with 0.1 M dopant. According to their different dopant ions Cl^-, TOS^-, and DBS^-, the composites were named as PPy-Cl/FSWNTs, PPy-TOS/FSWNTs, and PPy-DBS/FSWNTs, respectively. As a contrast, the composites without additional dopant were also electrochemically co-deposited in the dispersive solution of Py and FSWNTs, consequently, was called as pristine PPy/FSWNTs. The current density was 2 $mAcm^{-2}$ and the polymerization temperature was 4°C for all the preparations. After polymerization, the electrodes were cleaned twice with deionized water and

then dried for 12 h in a vacuum oven at the temperature of 100°C.

All electrochemical preparations and tests were done on the Versatile Multichannel Potentiostat 2/Z (VMP2, Princeton applied research) with the ability of impedance measurements. The electrochemical performance was investigated by using cyclic voltammetry (CV), galvanostatical charging–discharging and EIS techniques with 3 M KCl aqueous solution as electrolyte. In three-electrode system, a platinum sheet was used as the counter electrode and a saturated calomel electrode (SCE) as the reference electrode. Two-electrode system consisted of a pair of almost identical composite electrodes. EIS measurements were made in the frequency range from 100 kHz down to 10 mHz with an sinus voltage of 10 mV.

The mass of composites was determined by the electronic balance (AG 135, Mettler-Toledo, precision 0.01 mg). The morphology of samples was observed on Field Emission Scanning Electron Microscope (JSM-6700F, JEOL Ltd.). Energy dispersive X-ray spectroscopy (EDS) was obtained by high-performance Energy Dispersive Analysis System of X-ray (Oxford INCA). The Fourier transform infrared spectroscopy (FTIR) was measured on FTIR spectrometers (Bruker, VERTEX 70).The XPS spectra were obtained by Axis Ultra, Kratos (UK) using monochromatic Al K_α radiation (150 W, 5 kV, 1,486.6 ev). The vacuum in the spectrometer was 10^{-9} Torr.

Results and discussion

Figure 1 displays the morphology of pristine PPy/FSWNT, PPy-Cl/FSWNT, PPy-TOS/FSWNT, and PPy-DBS/FSWNT composites. PPy coated each individual FSWNT uniformly to form nanorod-like structures and binded the coated nanotubes together in a nanoporous three-dimensional (3D) network. The coated FSWNTs tend to align parallel to the plane of the electrode while maintaining random orientation [15]. Although the four kinds of composites had the nanorods with a length of around 100 nm, because of the template effect of FSWNTs with the length less than 100 nm [28], they exhibited differences in the diameter of the nanorods. The diameter of pristine PPy/FSWNT nanorods was only 20 nm and that of PPy-Cl/FSWNTs nanorods was around 50 nm from Fig. 1a, b. The diameter of PPy-TOS/FSWNT nanorods further increased to around 100 nm as shown by Fig. 1c, e. PPy-DBS/FSWNT composites became more compact, with only few nanorod-like structures left, as shown by Fig. 1d, f. The evolvement of the morphology may be related to the increasing surfactivity in the order of Cl^-, TOS^-, and DBS^-. The reason why PPy-DBS/FSWNT composites exhibited comparatively compact films with partly porous structure may be that the nanoporous structure previously constructed by the nanorods was partly filled up by PPy-DBS, since nanoporous structure within the composites is easy to access for the polymerization solution with the assistance of DBS, which is a good anionic surfactant.

PPy/FSWNT composites without other dopant can be electrochemically obtained because the anionic FSWNTs with oxygenated groups resulting from functionalization are able to act as the doping ions [24]. The existence of the oxygenated groups was confirmed by FTIR spectroscopy. EDS analysis revealed that the atom ratio of O/C reached 1/8 in the FSWNTs. If without functionalization process, in the dispersive solution of Py and SWNTs without other dopant, the surface of Ta electrode was electrochemically oxidized to inert films, rather than PPy/SWNT composite was electrochemically co-deposited.

Although the four kinds of composites had similar nanoporous 3D structures, they exhibited distinctly different capacitive behaviors. Figure 2a presents their CV curves with the polymerization charge of 7.2 Ccm^{-2}.

The output current of the PPy-TOS/FSWNT nanocomposite was significantly greater than that of the others. This indicates that PPy-TOS/FSWNT nanocomposite had the largest capacitance, since capacitance can be estimated from the output current divided by the scan rate. Furthermore, the CV curve of PPy-TOS/FSWNTs was very close to rectangle. There was almost no current delay observed in PPy-TOS/FSWNT electrodes during reversing the potential sweep, which suggests a very fast kinetic process [29]. In addition, its voltammetric charges on the positive and negative sweeps were approximately the same, implying a good electrochemical reversibility in the potential region of −400 to 500 mV (vs SCE). All of above signifies that PPy-TOS/FSWNT nanocomposites exhibited an ideal capacitance behavior. The CV curve of PPy-Cl/FSWNT nanocomposites was also close to rectangle, but its current response was obviously less than that of PPy-TOS/FSWNTs. As for PPy/FSWNT nanocomposites, the CV curve was in a shuttle-like shape, indicating a resistance behavior, while PPy-DBS/FSWNT nanocomposite had even hardly any output current.

The electrochemical capacitance properties of the four kinds of nanocomposites were also examined by galvanostatical charging–discharging technique. Their discharging curves at current load of 1 $mAcm^{-2}$ are shown in Fig. 3. The curves of PPy-TOS/FSWNTs and PPy-Cl/FSWNTs were linear in the whole range of potential without any obvious ohm-drop (IR-drop) phenomenon, which confirms an ideal capacitance behavior again. Their specific capacitances were 216 Fg^{-1} and 256 Fg^{-1}, based on their actual weights of electrode material of 3.61 and 2.45 mg, respectively. In contrast, PPy/FSWNT composite displayed a terribly distinct IR-drop, with the potential dropping from

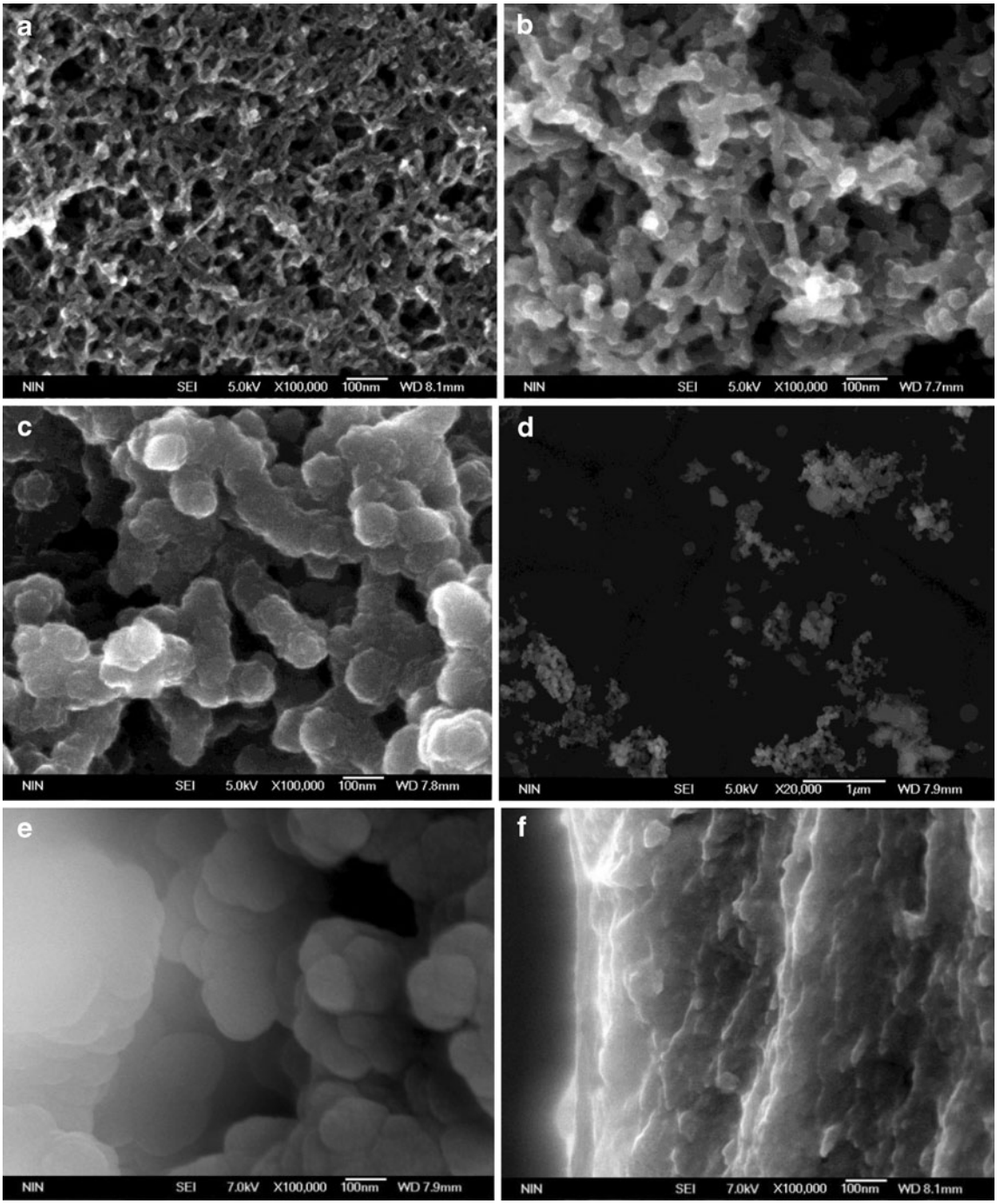

Fig. 1 Surface morphology of pristine PPy/FSWNTs (**a**), PPy-Cl/FSWNTs (**b**), PPy-TOS/FSWNTs (**c**), and PPy-DBS/FSWNTs (**d**); cross-section morphology of PPy-TOS/FSWNTs (**e**) and PPy-DBS/FSWNTs (**f**)

0.5 to 0 V (vs SCE) at the beginning of the discharging process, as shown in the lower-left corner of Fig. 3. Besides, its specific capacitance was as low as 17 Fg^{-1}, based on the actual mass of electrode material of 1.41 mg. Although PPy-DBS/FSWNTs had no obvious ohm-drop phenomenon, the discharging curve deviated far from linear, indicating a serious activation polarization. Consequently, PPy-DBS/FSWNTs had a very low specific capacitance, only 0.185 Fg^{-1}, according to the mass of 6.71 mg.

Compared with PPy-Cl/FSWNTs, PPy-TOS/FSWNT nanocomposites had higher capacitance, but had a slightly lower specific capacitance, because PPy-TOS/FSWNTs had greater mass when prepared with the equal polymerization charge. The difference in their mass mainly came from that they had approximate doping level (around 0.3), and the

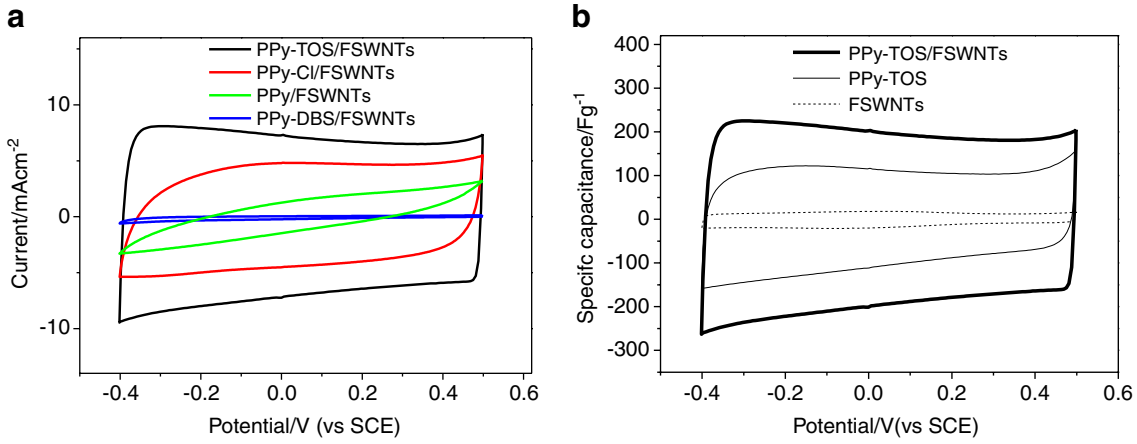

Fig. 2 CV curves of pristine PPy/FSWNT, PPy-Cl/FSWNT, PPy-TOS/FSWNT, and PPy-DBS/FSWNT nanocomposites (**a**); CV curves (current was displaced by specific capacitance) of PPy-TOS/FSWNT, PPy-TOS and FSWNT (**b**); tested at a scanning rate of 10 mVs^{-1} in 3 M KCl solution

mole mass of TOS^- (172 $gmol^{-1}$) is much greater than that of Cl (35.5 $gmol^{-1}$). If based on the mass of PPy only calculated from the polymerization charge, the specific capacitance of PPy-TOS/FSWNTs was up to 326 Fg^{-1}, which is significantly greater than that of PPy-Cl/FSWNTs, i.e., 280 Fg^{-1}. From a practical point of view, it is useful to complement the mass specific capacitance (C_M, Fg^{-1}) by area specific capacitance (C_A, Fcm^{-2}) [11]. The C_A of PPy-TOS/FSWNT nanocomposite reaches 0.78 Fcm^{-2} from Fig. 3 and that of PPy-Cl/FSWNTs nanocomposite is markedly lower, 0.64 Fcm^{-2}, whereas the C_A of pristine PPy/FSWNTs is merely 0.024 Fcm^{-2}, and that of PPy-DBS/FSWNTs is even barely 0.0013 Fcm^{-2}.

From the above discussion, a conclusion can be drawn that PPy-Cl/FSWNT and PPy-TOS/FSWNT nanocomposites exhibited ideal capacitive behaviors with high C_M and C_A, whereas pristine PPy/FSWNT and PPy-DBS/FSWNT nanocomposites had very low electrochemical activity. The reason was examined by using EIS technique, a powerful tool to study the electrochemical process of electrodes and to evaluate their electronic and ionic conductivities. The results are shown by Fig. 4. As for pristine PPy/FSWNTs, two well-separated patterns are observed: an arc at high-frequency region, which is related to interfacial processes; a line which is almost perpendicular to the real axis at low-frequency region, indicating a capacitive behavior. The electrochemical charge transfer resistance (R_{CT}), which arises from a kinetically controlled electrochemical reaction including electron resistance of electrode material, ionic resistance, and an electron transfer between the electrode and the electrolyte, can be evaluated from the difference in the real part of the impedance between low and high frequencies. The R_{CT} value of pristine PPy/FSWNTs was as great as 280 ohm because PPy on the surface of the composite had a low electronic conductivity resulted from low doping level, which will be revealed later by XPS analysis. It was the high R_{CT} that resulted in the pristine PPy/FSWNT electrode having a large IR-drop in the discharging curve (as shown by Fig. 2) and consequently a low capacitance.

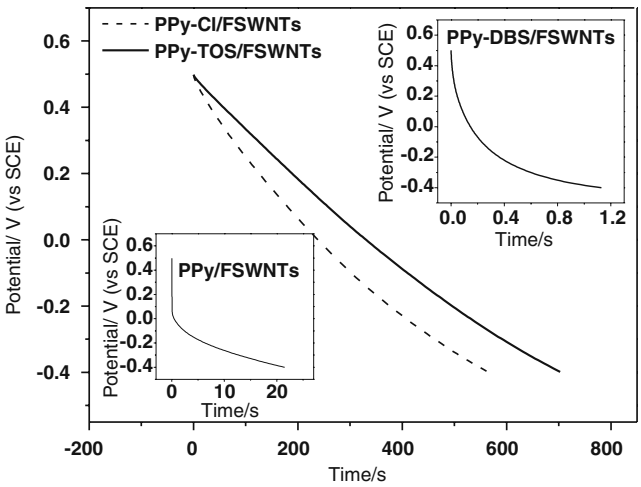

Fig. 3 Galvanostatical discharging curve of pristine PPy/FSWNT, PPy-Cl/FSWNT, PPy-TOS/FSWNT, and PPy-DBS/FSWNT nanocomposites tested at a current density of 1 $mAcm^{-2}$

As for PPy-Cl/FSWNT and PPy-TOS/FSWNT nanocomposites, their R_{CT} values were even lower than 0.05 ohm, which is remarkably smaller than that of pristine PPy/FSWNTs. This can be explained by the high conductivity of PPy coatings with appropriate doping level in PPy-Cl/FSWNT and PPy-TOS/FSWNT nanocomposites. Accordingly, there was no obvious IR-drop in their discharging curves, as shown by Fig. 3. Even at the state of deep charging (0.5 V vs SCE) and deep discharging (−0.4 V vs SCE), all the R_{CT} values of PPy-Cl/FSWNT and PPy-TOS/

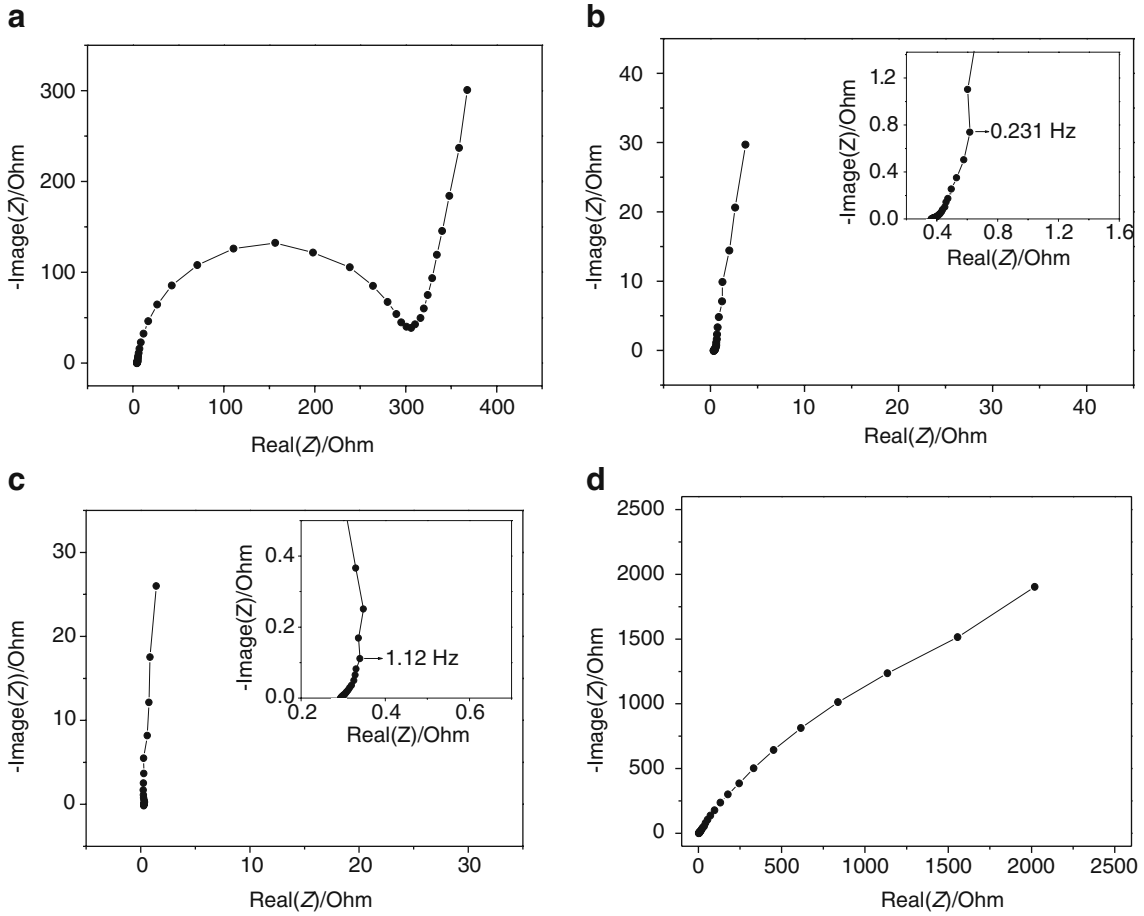

Fig. 4 EIS spectra of pristine PPy/FSWNTs (**a**), PPy-Cl/FSWNTs (**b**), PPy-TOS/FSWNTs (**c**), and PPy- DBS/FSWNTs (**d**) tested at the open circuit potential in 3 M KCl solution

FSWNT nanocomposites were less than 1 ohm, which agree well with the rectangle-like shape of their CV curves. The imaginary parts of the impedance of PPy-Cl/FSWNT and PPy-TOS/FSWNT nanocomposites in the low-frequency area were almost perpendicular to their real parts, indicating an ideal capacitance behavior. On the other hand, PPy-TOS/FSWNT nanocomposites exhibited a much higher knee-frequency, i.e., the maximum frequency at which capacitive behavior can be predominantly maintained, which confirms a fast charging–discharging rate once more. The capacitance of PPy-TOS/FSWNT and PPy-Cl/FSWNT nanocomposites calculated from EIS at frequency of 10 mHz were 0.612 and 0.536 F, respectively, which are slightly smaller than the values calculated from the CV curves and galvanostatical discharging curves due to the redox switching hysteresis of conducting polymer [30].

As for PPy-DBS/FSWNTs, a bias related to the Warburg impedance behavior appeared in the low-frequency region, as shown by Fig. 4b. With its large size, DBS^- is embedded in the PPy matrix and difficult to exchange with Cl^- in the solution during the charging–discharging process, which consequently obstructs the Cl^- in the electrolyte from entering the nanocomposites according to Donnan exclusion principle [31]. The obstructing effort brought on a high activation polarization and a very low specific capacitance.

PPy in pristine PPy/FSWNTs was also doped by the large anion FSWNT, but PPy/FSWNT composites had a comparatively higher capacitance than PPy-DBS/FSWNTs did. The reasons may be as the following: first, the shorter path lengths of anions transport in pristine PPy/FSWNTs due to its highly nanoporous structures, and the smaller nanorods (as shown by Fig. 1) permitted operation with low ionic conductivity [32]; second, the shorter path length for electronic transport due to the PPy coating with the thickness of only 10 nm on FSWNTs complemented the low electronic conductivity of PPy; third, the anionic FSWNTs, which was the center of pristine PPy/FSWNT nanorods, could not hinder the anions entering the outer-layer PPy. These can also be used to explain that pristine PPy/FSWNT exhibits capacitive behavior in low-frequency region. The high electrochemical activity of PPy doped by large-size anion can also be achieved when the charge

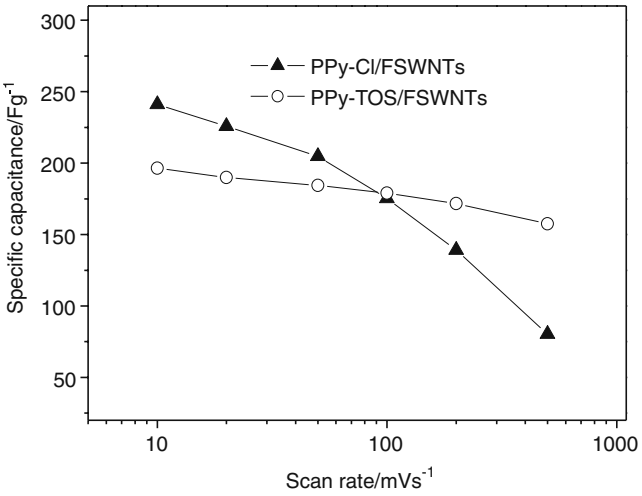

Fig. 5 Specific capacitance of PPy-Cl/FSWNTs and PPy-TOS/FSWNTs nanocomposites as function of scanning rate tested in 3 M KCl solution

balancing comes from the smaller cations in the electrolyte [33]. But the participation of cations generally happened at the more negative potential than −0.4 V (vs SCE) [34].

To further investigate their fast ion exchange performance, the electrochemical capacitance of PPy-TOS/FSWNT and PPy-Cl/FSWNT nanocomposites was tested by CV technique at various scanning rates, and the results are displayed in Fig. 5. At the scanning rate of 10 mVs^{-1}, their C_M values are 196 and 241 Fg^{-1}, respectively. The value of the PPy-TOS/FSWNTs remained smaller than that of PPy-Cl/FSWNTs nanocomposites when the scanning rate is less than 100 mVs^{-1}, however, the C_M value of the former had a weaker dependence on scanning rate and turned greater than that of the latter when the scanning rate exceeds 100 mVs^{-1}. Interestingly, the C_M value of PPy-TOS/FSWNTs was as high as 160 Fg^{-1} at 500 mVs^{-1} (namely a discharging time of 1.6 s), while that of PPy-Cl/FSWNTs was only 80 Fg^{-1}. Furthermore, the area specific of the former was three times higher that of the latter at

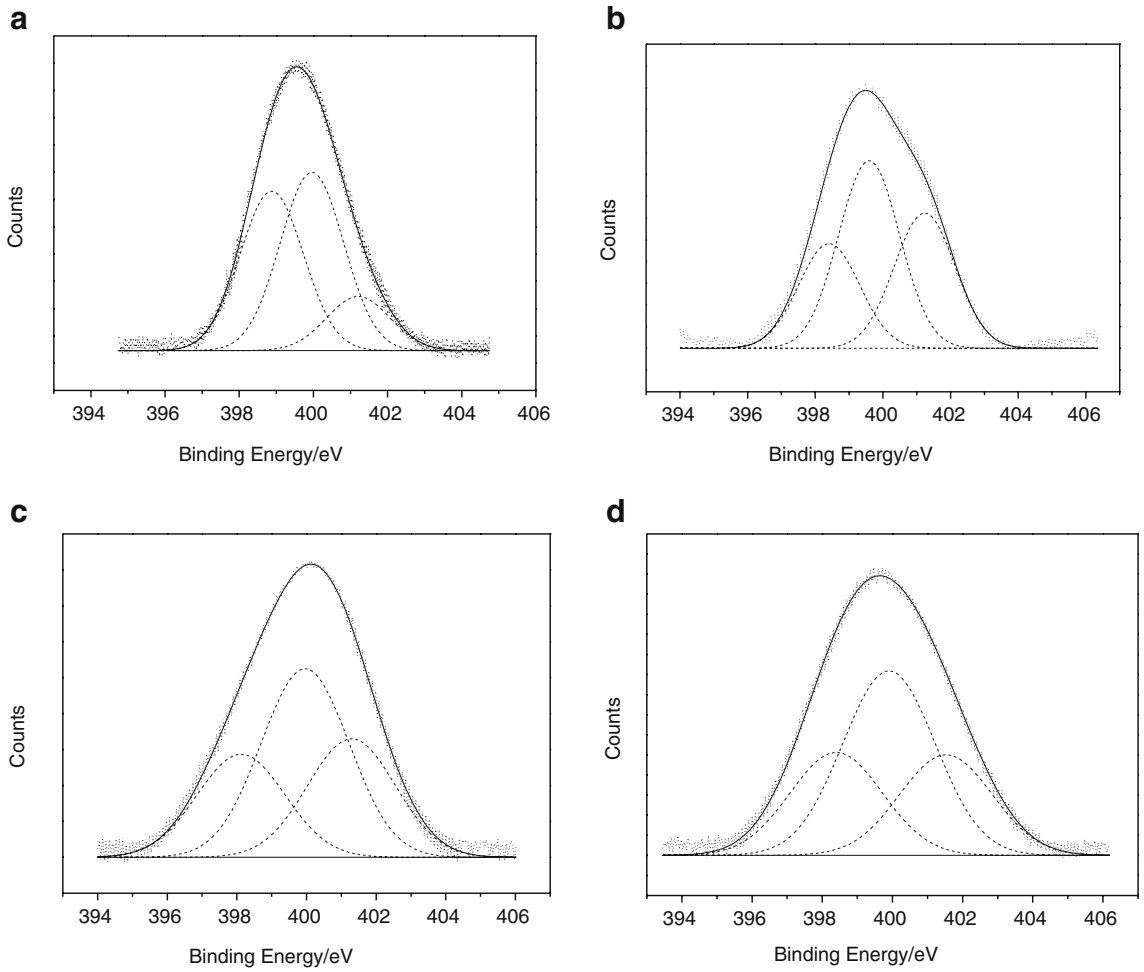

Fig. 6 Nitrogen 1 s XPS core-level spectra of the pristine PPy/FSWNTs (**a**), PPy-Cl/FSWNTs (**b**), PPy-TOS/FSWNTs (**c**), and PPy-DBS/FSWNTs (**d**); *Dot*: the measure curve, *Dash* line: the Gaussian curve, *solid line*: the integrated curve of the Gaussian curves

Table 1 Dependence of the doping level and defect density of PPy/FSWNTs on the dopants

Dopants	Doping level	Density of defects
FSWNTs	0.131	0.401
Cl^-	0.314	0.246
TOS^-	0.303	0.231
DBS^-	0.264	0.253

500 mVs^{-1}. Once again, it is illuminated that PPy-TOS/FSWNT nanocomposites had more rapid charging–discharging ability than PPy-Cl/FSWNTs did. What's more, the former had much higher mass specific capacitance at high charging–discharging rates, which is crucial for application in supercapacitors.

The high specific capacitance and very fast charging–discharging ability of PPy-TOS/FSWNT nanocomposites is inevitably related with its nanostructure ensuring sufficient surface area and its accessibility for the electrolyte [31] and the synergic effect of FSNWT and PPy. The synergic effect was demonstrated by the greater specific capacitance of PPy-TOS/FSWNTs than those of FSWNTs (around 30 Fg^{-1}) and PPy-TOS (around 150 Fg^{-1}), as shown by Fig. 2b, where current (i) in the CV plots was replaced by specific capacitance ($is^{-1}m^{-1}$, s represents the scanning rate and m is the mass of the electrode active material). However, the faster charging–discharging rate of PPy-TOS/FSWNTs than that of PPy-Cl/FSWNTs, even though the latter had a shorter path of electrons/ions transport due to the thinner PPy coating on FSWNTs, indicates that the dopants played a key role in fast charging–discharging performance. One possible reason why PPy-TOS/FSWNTs exhibited faster charging–discharging ability than PPy-Cl/FSWNTs did may be that a larger channel can be produced in the former when TOS^-, larger in size compared with Cl^-, ejected from the composite.

The electrochemical performance of PPy is also linked to its intrinsic structure, including the distribution of quinonoid imine (=N-), benzenoid amine (-NH-), positively charged nitrogen with protonation (-NH^+-) [10].

The effects of doping anions on the structure of PPy in the four kinds of nanoncomposites were quantitatively illustrated by examining their XPS core-level spectra. Their typical XPS core-level spectra of N 1 s are presented by Fig. 6. These core-level spectra show relatively broad peaks, which indicate the existence of several structures. Hence, the peaks were reasonably decomposed into three Gaussian peaks with the binding energy of 398.4, 399.9, and 401.2 eV, respectively. Among the three peaks, the lowest binding energy peak related to the imine-like structure (>C=N-) can be used to estimate the density of defects within the PPy [35] because the structrure is considered to interrupt the electron hopping on the polymer chain [36]. The peak at 399.9 eV is owing to the amine-like structure (-NH-) [37]. The peak with the highest binding energy is caused by the positively charged N atoms with protonation (-NH^+-) [38]. Consequently, the effect of dopant on the doping level and the defect density of PPy can be quantitatively estimated. The former was calculated from the ratio of the area of peak at 401.2 eV to the total area of the N 1 s peak and the latter from the ratio of the 398.4 eV component to the same area. These results are presented in Table 1.

The doping level of pristine PPy/FSWNTs was only 0.131, and the density of defects was up to 0.401, which resulted in its low electronic conductivity. More or less, Cl^-, TOS^-, and DBS^- can help to increase the doping level and to reduce defect density. The doping level of PPy in PPy-Cl/FSWNT composite was 0.314, and the density of

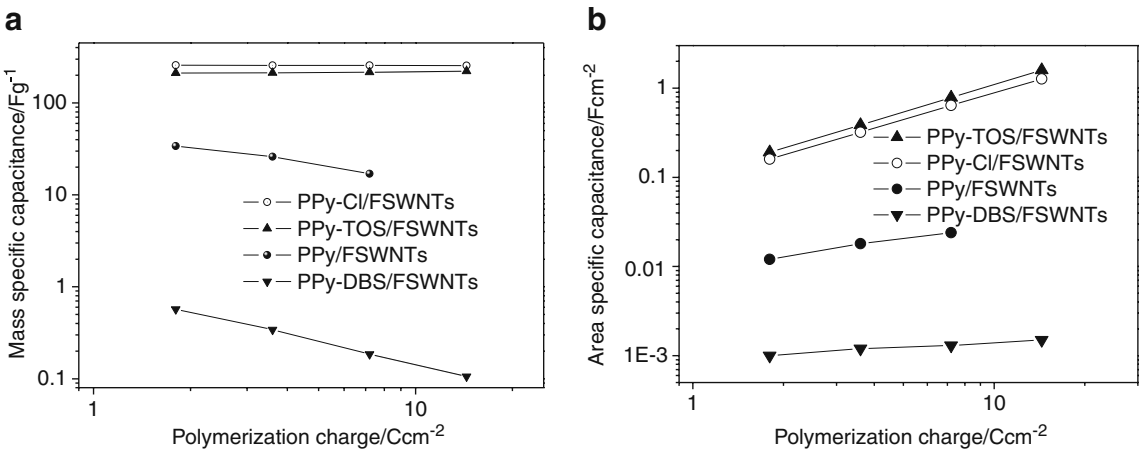

Fig. 7 Mass specific capacitance (**a**) and area specific capacitance (**b**) of PPy/FSWNT, PPy-Cl/FSWNT, PPy-TOS/FSWNT, and PPy-DBS/FSWNT nanocomposites with various polymerization charge tested in 3 M KCl solution at a current load of 1 m Acm^{-2}

defects was 0.246, which agrees well with the value reported by Hu et al. [10]. PPy-TOS/FSWNTs had even lower defect density, which may be another reason that it had higher capacitance and faster charging–discharging rate. As for PPy-DBS/FSWNTs, its doping level was the smallest in the three none-pristine composites, and it may be caused by its large dopants DBS^{-}.

The effect of thickness on the capacitance properties of the four kinds of nanocomposites was examined to further illustrate their ion transport behavior during charging–discharging process. Figure 7a presents the C_M values of the four kinds of nanocomposites with polymerization charge of 1.8, 3.6, 7.2, and 14.4 Ccm^{-2}, where current load was 1 m Acm^{-2}. Generally speaking, mass specific capacitance of polymer electrodes invariably decrease with the increase of the thickness (polymerization charge), apparently because of the longer ionic transport route and the low ionic mobility within the solid polymer. As a result, a large specific capacitance of such electrodes was accessible only in thin films (such as, polymerization equal to or less than 1 Ccm^{-2}) [10].

However, the C_M value of PPy-TOS/FSWNT and PPy-Cl/FSWNT nanocomposites did not decrease when polymerization charge changed from 1.8 to 14.4 Ccm^{-2}. Therefore, the C_A values of PPy-TOS/FSWNT and PPy-Cl/FSWNT nanocomposites increased linearly with the polymerization charge as shown in Fig. 7b. The value of PPy-TOS/FSWNTs, especially, was up to 1.6 Fcm^{-2} at polymerization charge of 14.4 Ccm^{-2}.This can be attributed to the retaining nanoporous structures in the thick films which provided enough paths for the movement of ions and solvent molecules, resulting in the improved electrochemical properties. By comparison, the C_M value of PPy/FSWNTs decreased obviously with the increase of thickness, which should be related to the low electronic conductivity of the nanocomposite, although the nanocomposite had also highly nanoporous structure like PPy-TOS/FSWNTs as shown by Fig. 1. From Fig. 7a, the C_M value of PPy-DBS/FSWNTs decreased sharply with the increase of polymerization charge (thickness), and the C_A value hardly increased with the increase of polymerization charge, as shown in Fig. 7b. This indicates only the surface of PPy-DBS/FSWNTs having electroactivity, agreeing with its result of EIS analysis.

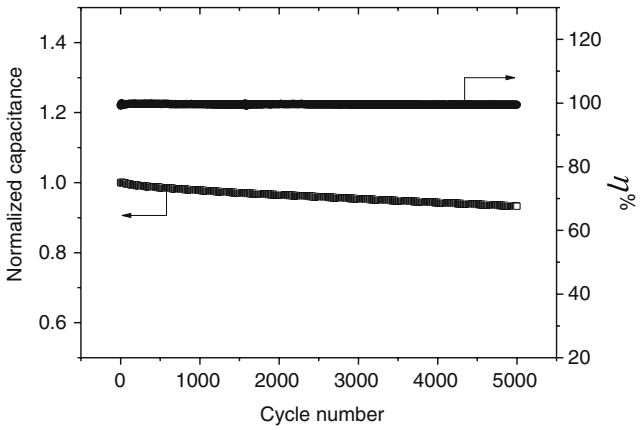

Fig. 9 The normalized capacitance and coulombic efficiency of PPy-TOS/FSWNT nanocomposites during the cycle in two-electrode system at a current load of 1.2 Ag^{-1} in 3 M KCl solution

A slightly increase in the C_M value of PPy-TOS/FSWNT nanocomposites with the increase of the film thickness is observed from Fig. 7a, which may be related to the reducing of discharging rate in thicker films. The electrochemical capacitance of PPy-TOS/FSWNTs with various polymerization charges was further tested by using CV technique at the scanning rate of 10 mVs^{-1}, and the results are exhibited in Fig. 8. Every CV curve exhibited a satisfactory rectangular shape, as shown in Fig. 8a. On

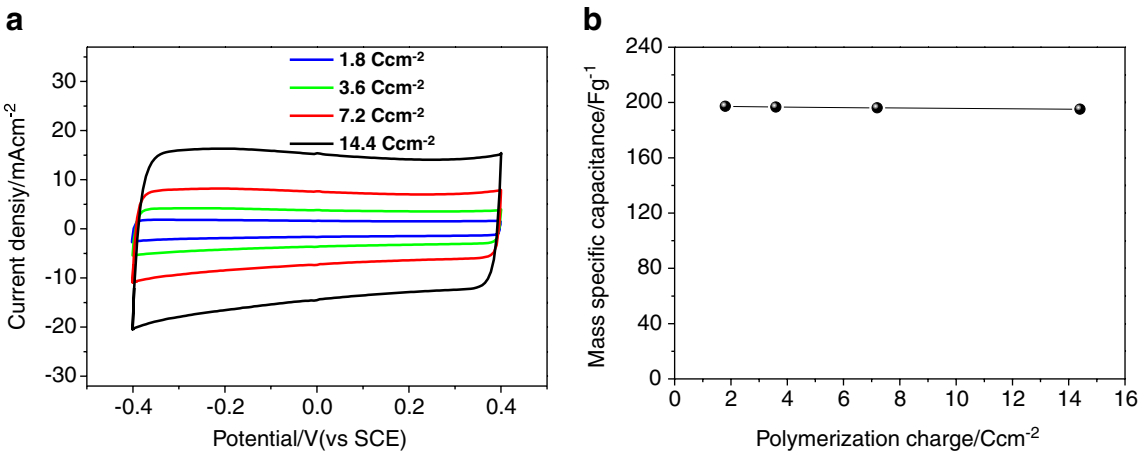

Fig. 8 CV curves at scanning rate of 10 mVs^{-1} (**a**) and mass specific capacitance (**b**) of PPy-TOS/FSWNT nanocomposites with various polymerization charge tested in 3 M KCl solution

reversing the potential at both positive and negative ends, the current switching was very fast as indicated by the almost vertical lines in the figure. This suggests the thick PPy-TOS/FSWNT composite films, even with polymerization charge up to 14.4 Ccm^{-2}, still display a very good capacitive behavior, which can be attributed to their high electron conductivity and the existence of favorable ion transport channels. Furthermore, the mass specific capacitance of PPy-TOS/FSWNT nanocomposites, as shown in Fig. 8b, did not decrease when polymerization charge changed from 1.8 to 14.4 Ccm^{-2}, which agrees well with the results of galvanostatical charging–discharging tests.

To evaluate the applicability of PPy-TOS/FSWNTs in supercapacitors further, the cycling performance and coulombic efficiency (discharging capacitance divided by charging capacitance) of PPy-TOS/FSWNT nanocomposites in two-electrode system were tested by the galvanostatical charging–discharging with a potential window of 0.8 V at a current load of 1.2 Ag^{-1}. PPy-TOS/FSWNT nanocomposites exhibited very stable cycling performance, and its capacitance can retain 93.2% after 5,000 cycles as shown by Fig. 9. The excellent cycling stability may be attributed to the strain of Cl^- (in the testing electrolyte) insertion/ejection being accommodated by FSWNTs and nanostructure in the composites. On the other hand, the coulombic efficiency of PPy-TOS/FSWNT nanocomposites reached 99.5% because the nanocomposites had low ionic and electronic resistance, as shown by Fig. 4.

Conclusions

Uniform PPy/FSWNTs composites doped with FSWNTs, Cl^-, TOS^-, and DBS^-, respectively, were electrochemically co-deposited in the suspension solution of FSWNTs. The nature of dopant anions of PPy significantly affected the morphology and capacitance characteristics of the resultant nanocomposites. Their mass specific capacitance (C_M) at the scanning rate of 10 mVs^{-1} was in the order of PPy-Cl/FSWNTs > PPy-TOS/FSWNTs ≫ pristine PPy/FSWNTs ≫ PPy-DBS/FSWNTs, where the sign ≫ means much greater.

PPy-DBS/FSWNT nanocomposites had hardly any electrochemical activity mainly because DBS^-, with its overlarge size, was embedded in PPy matrix and consequently, battled the anions exchange during charging–discharging process. Besides, since DBS has great surfactivity, the nanoporous structure of the nanocomposites was partly filled up by PPy-DBS. The poor C_M of PPy/FSWNT nanocomposites resulted from the low electronic conductivity of PPy due to the low degree of doping and high density of defects. Thanks to the appropriate size of dopant and the lowest density of defect in the PPy-TOS, PPy-TOS/FSWNT nanocomposites presented the highest area specific capacitance and fastest charging–discharging behavior. Its C_M was slightly less than that of PPy-Cl/FSWNTs at low scanning rates due to the greater mass of its dopant TOS^-, but greater in the condition of fast charging–discharging process (when scanning rate >100 mVs^{-1}), which satisfies a crucial requirement of application in supercapacitors. It was also found that PPy-TOS/FSWNT nanocomposites had an excellent cycling performance with high stability and coulombic efficiency. All the results reveal that dopants played an important role in the capacitance, fast charging–discharging ability and cycling performance of PPy/FSWNT nanocomposites. In addition, PPy-TOS/FSWNT nanocomposite was demonstrated to be a kind of excellent electrode material for supercapacitors.

Acknowledgements The authors thank for the financial supports by the National High Technology Research and Development Program of China (Grant No. 2007AA03Z249) and the National Natural Science Foundation of China (Grant No. 20804030).

References

1. Conway BE (1999) Electrochemical supercapacitors: scientific fundamentals and technological applications. Kluwer/Plenum, New York
2. Mastragostino M, Soavi F (2007) J Power Sources 174:89
3. Miller JR, Simon P (2008) Science 321:651
4. Li W, Chen J, Zhao J, Zhang J, Zhu J (2005) Mater Lett 59:800
5. Xu YL, Wang J, Sun W, Wang SH (2006) J Power Sources 159:370
6. Wang J, Xu YL, Chen X, Du XF (2007) J Power Sources 163:1120
7. Winter M, Brodd RJ (2004) Chem Rev 104:4245
8. Fan L-Z, Maier J (2006) Electrochem Commun 8:937
9. Song SH, Han DS, Lee HJ, Cho HS, Chang SM, Kim JM, Muramatsu H (2001) Synth Met 117:137
10. Hu CC, Lin XX (2002) J Electrochem Soc 149:A1049
11. Ingram MD, Staesche H, Ryder KS (2004) J Power Sources 129:107
12. Groenendaal BL, Jonas F, Freitag D, Pielartzik H, Reynolds JR (2000) Adv Mater 12:481
13. Chen GZ, Shaffer MSP, Coleby D, Dixon G, Zhou WZ, Fray DJ, Windle AH (2000) Adv Mater 12:522
14. Jurewicz K, Delpeux S, Bertagna V, Beguin F, Frackowiak E (2001) Chem Phys Lett 347:36
15. Hughes M, Chen GZ, Shaffer MSP, Fray DJ, Windle AH (2002) Chem Mater 14:1610
16. Ham HT, Choi YS, Jeong N, Chung IJ (2005) Polymer 46:6308
17. Frackowiak E, Khomenko V, Jurewicz K, Lota K, Beguin F (2006) J Power Sources 153:413
18. Wang J, Xu YL, Chen X, Sun XF (2007) Comp Sci Tech 67:2981
19. Lin XQ, Xu YH (2008) Electrochim Acta 53:4990
20. Kim JY, Kim KH, Kim KB (2008) J Power Sources 176:396
21. Fan JH, Wan MX, Zhu DB, Chang BH, Pan ZW, Xie SS (1999) Synth Met 102:1266
22. Lota K, Khomenko V, Frackowiak E (2004) J Phys Chem Solids 65:295
23. Hughes M, Shaffer MSP, Renouf AC, Singh C, Chen GZ, Fray J, Windle AH (2002) Adv Mater 14:382
24. Peng C, Jin J, Chen GZ (2007) Electrochim Acta 53:525

25. Liu J, Rinzler AG, Dai HJ, Hafner JH, Bradley RK, Boul PJ, Lu A, Iverson T, Shelimov K, Huffman CB, Rodriguez-Macias F, Shon YS, Lee TR, Colbert DT, Smalley RE (1998) Science 280:1253
26. Tasis D, Tagmatarchis N, Bianco A, Prato M (2006) Chem Rev 106:1105
27. Wang J, Xu YL, Chen X, Du XF, Li XF (2007) Acta Phys-Chim Sin 23:299
28. Wang J, Xu YL, Sun XF, Li XF, Du XF (2008) J Solid State Electrochem 12:947
29. Ghosh S, Inganas O (1999) Adv Mater 11:1214
30. Hass R, García-Cañadas J, Garcia-Belmonte G (2005) J Electroanal Chem 577:99
31. Wang J, Xu YL, Sun XF, Mao SC, Xiao F (2007) J Electrochem Soc 154:C445
32. Arico AS, Bruce P, Scrosati B, Tarascon JM, Van Schalkwijk W (2005) Nat Mater 4:366
33. Naoi K, Oura Y, Maeda M, Nakamura S (1995) J Electrochem Soc 142:417
34. Skaarup S, West K, Gunaratne LMWK, Vidanapathirana KP, Careem MA (2000) Solid State Ion 136:577
35. Joo J, Lee JK, Lee SY, Jang KS, Oh EJ, Epstein AJ (2000) Macromolecules 33:5153
36. Ribo JM, Dicko A, Tura JM, Bloor D (1991) Polymer 32:728
37. Kang ET, Neoh KG, Ong YK, Tan KL, Tan BT (1991) Macromolecules 24:2822
38. Cairns DB, Armes SP, Chehimi MM, Perruchot C, Delamar M (1999) Langmuir 15:8059